Supporting Information

Interfacial Redox Catalysis on Gold Nanofilms at Soft Interfaces

Evgeny Smirnov,[a] *Pekka Peljo,*[a] *Micheál D. Scanlon,*[a,b] *and Hubert H. Girault*[a]*.

[a]Laboratoire d'Electrochimie Physique et Analytique, Ecole Polytechnique Fédérale de Lausanne, Station 6, CH-1015 Lausanne, Switzerland.

[b]Department of Chemistry and the Tyndall National Institute, University College Cork, Cork, Ireland.

Table of Contents

SI-1. Nanoparticle characterization

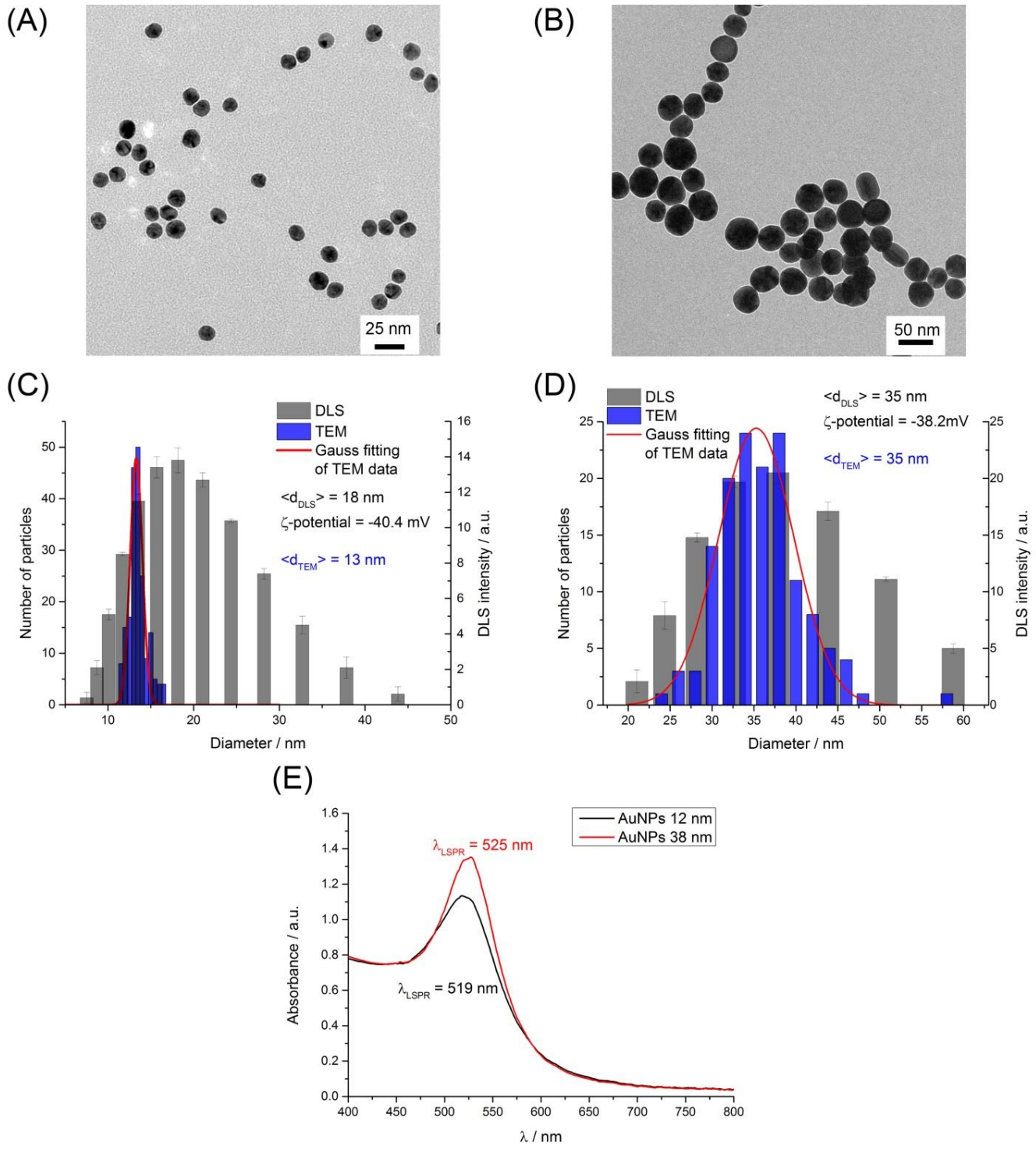

Figure S1. *Characterization of the as-synthesized citrate stabilized AuNPs, with two mean diameters (A, C) 12 nm and (B, D) 38nm, by TEM, DLS and UV/Vis spectroscopy.*

The morphologies of the AuNPs in each colloidal solution were examined by **Transmission Electron Microscopy** (**TEM**, Figures S1A and B). The as-prepared AuNP solutions were dropped onto standard

carbon-coated copper grids (200-mesh) and air-dried for about two hours. The TEM images were obtained using a FEI CM12 (Philips) transmission electron microscope, operating with a LaB_6 electron source at 120 kV. The average size distributions of the AuNPs, with an assumption made that the AuNPs were perfect spheres, were determined on the basis of the TEM images with the use of ImageJ software. For each sample 4-5 individual TEM images were analyzed by ImageJ, gathering information from more than 150 AuNPs. The mean diameters (d / nm) of the smaller and larger AuNPs were 13 ± 1 nm and 35 ± 10 nm, respectively (Figures S1A and B).

Zeta(ζ)-potential and Dynamic Light Scattering (DLS) measurements were carried out on a Nano ZS Zetasizer (Malvern Instruments, U.K.), with irradiation (λ = 633 nm) from a He-Ne laser, using Dispersion Technology Software (DTS). The AuNP samples (approximately 0.75 mL) were injected into a folded capillary cell. The ζ-potential (mV) was elucidated from the measured electrophoretic mobility using the Smoluchowski approximation of Henry's equation. DLS measures Brownian motion and relates the particles speed to its size using the Stokes-Einstein equation. The AuNPs were illuminated with the laser and the intensity fluctuations of the scattered light analyzed. All particle size measurements were carried out at 25 °C and a 2 min equilibration time was employed. In comparison to the TEM result, DLS shows a bigger mean diameter for the smaller AuNPs (18 nm for DLS *versus* 13 nm form TEM analysis) and wider size distributions for both AuNP solutions (Figures S1C and S1D). This is normal and caused by the inherent nature of the method which measures the hydrodynamic radius. The latter is typically higher for smaller particles due to relatively larger contribution of the charged shells.

An alternative method of determining the mean diameters and the number density (N_{AuNPs}) of AuNPs in the colloidal solutions was to employ UV/vis spectroscopy, as detailed by Haiss *et al.*[1] and summarized by Smirnov *et al.*[2] UV/Vis spectra were obtained on a Perkin Elmer Lambda XLS+ spectrophotometer using a polystyrene cell with an optical path length of 1 cm (Figure S1E). Several critical parameters, such as the wavelength and absorbance of the experimentally observed localized surface plasmon resonance (LSPR) extinction peak (λ_{LSPR} and A_{LSPR}) and the absorbance at 450 nm (A_{450}), were obtained from these spectra and the mean diameters determined as 12 and 38 nm for the smaller and larger AuNPs, respectively, in excellent agreement with the TEM and DLS measurements. N_{AuNPs} was estimated as $4.0 \cdot 10^9$ particles/μL and $1.1 \cdot 10^8$ particles/μL for the 12 and 38 nm AuNPs, respectively.

SI-2. In situ monitoring of the interfacial AuNP nanofilm formation process

Movie S1. This movie shows the formation of the interfacial AuNP nanofilm *via* precise microinjection of colloidal 38 nm AuNPs suspended in methanol to the vicinity of the interface, with the snapshots of the movie shown in Figure S2. The purpose of this video is to demonstrate the *in situ* nanofilm formation process and the appearance of the mirror-like reflection from the nanofilm with increasing interfacial AuNP concentrations.

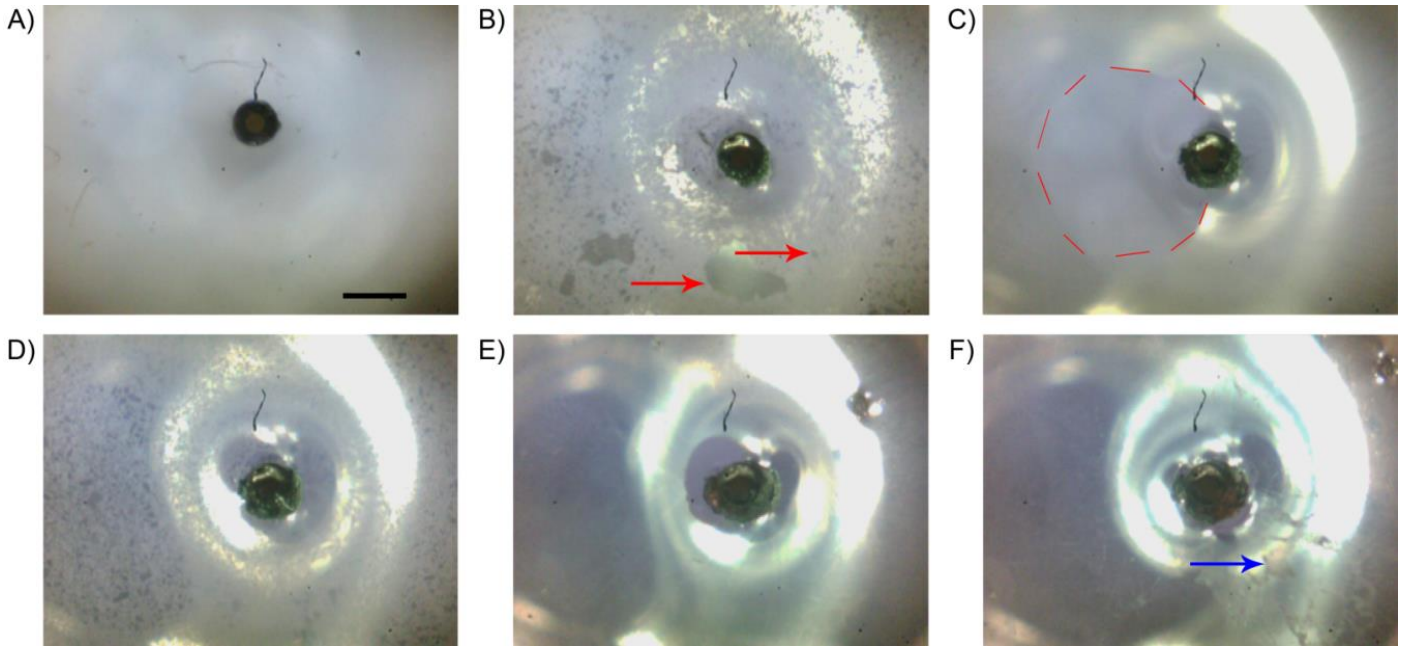

Figure S2. *Interfacial AuNP Film formation process captured in snapshots from Movie S1.* ***(A)*** *Image of a pure water | trifluorotoluene (TFT) interface with a silica capillary attached to the interface and held in place by capillary forces.* ***(B)*** *Image taken after 5 µL of the methanol solution of AuNPs was injected and the flow stopped; the red arrows indicate the positions of small and big islands.* ***(C)*** *Image taken during continuous methanol injection; an area free of AuNPs is shown by the red dashed curve.* ***(D)*** *Image taken after 10 µL of the methanol solution of AuNPs was injected and the flow stopped.* ***(E-F)*** *Images before and after the critical point, where cracks and wrinkles (blue arrow) started to form. Scale bar is equal to 0.5 mm*

The *in situ* AuNP film formation process passes through several different stages. Initially, tiny "islands" of AuNP aggregates were observed at the interface (Figure S2B). The interface itself was disturbed by the flow of solution from the capillary and, therefore, these small islands of AuNPs were very mobile at the interface (Figure S2C). This constant motion caused any relatively large aggregates of AuNPs to break apart, although the majority of the smaller islands of AuNPs remained intact. Thus, in the middle of the

interfacial AuNP film formation process, numerous randomly distributed small islands were present and weakly connected to each other (Figure S2D). However, as the interfacial concentration of AuNPs increased, a consistent reflective interfacial AuNP film appeared (Figure S2E). If excess solution containing AuNPs suspended in methanol was added, wrinkles and cracks appeared in the interfacial AuNP film (Figure S2F).

SI-3. Scanning electron microscopy (SEM) of the interfacial 38 nm AuNP nanofilms

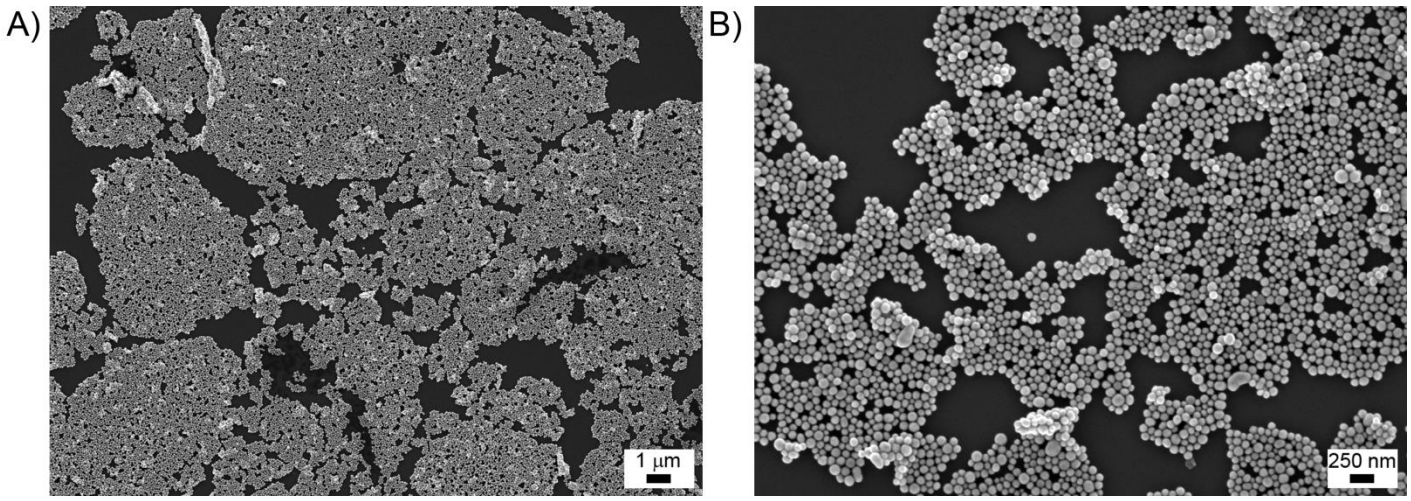

Figure S3. *SEM-images of prepared AuNP assembly with mean diameter of 38 nm at water*│*TTF interface.*

The morphologies and packing arrangement of the interfacial AuNP nanofilms formed with the larger (38 nm) AuNPs were investigated by SEM (Figure S3). AuNPs were carefully transferred to a silicon substrate. The smooth silicon substrate was treated with oxygen plasma (Diener Femto Plasma System) for 15 minutes prior to film transfer. This both ensured maximum cleanliness of the surface and the presence of a hydrophilic SiO_2 layer. The hydrophilicity of the SiO_2 layer was crucial to ensure that the hydrophilic liquid gold film transferred to the solid substrate without complications. As discussed in the main text, the packing arrangements consisted of randomly distributed close-packed assemblies or "islands" of AuNPs interspersed with voids of various sizes.

SI-4. Control experiments and electrochemical analysis

SI-4A: Control experiments

0.1 mL of methanol, 1 % (v/v) sodium citrate and ascorbic acid were separately added to a "blank" electrochemical cell containing only supporting electrolytes (see Cell 1 in Scheme 4B, main text). Each of these species were added at concentration levels at least one order of magnitude higher than those used in the preparation of the AuNPs and, as shown in Figure S4, had no major influence on the polarizable potential window. As noted in the main text, additional ITs events were observed at positive and negative potentials for the interfacial film consisting of 38 nm AuNPs and attributed to the transfers of Ag^+ and NO_3^- or other residuals left over from the synthesis of these NPs, respectively.

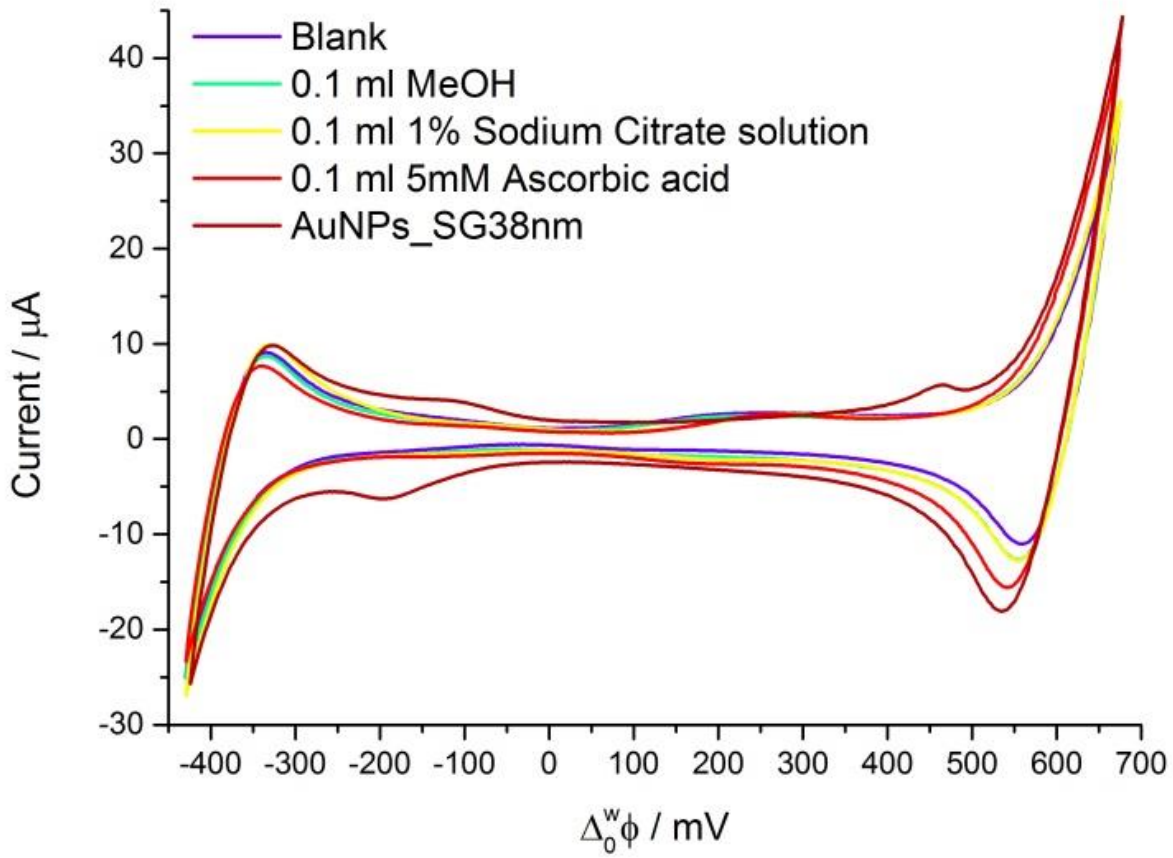

Figure S4. *Influence of possible interfering chemical species on the IT transfer voltammetry at a water | TFT interface for a "blank" electrochemical cell (see Scheme 4B, main text). Scan rate: 25 mV* s^{-1}.

SI-4B. Randles-Ševčík analysis

The Randles-Ševčík equation links the bulk concentration of a charged species c_{bulk} with the maximum peak current I_p arising from IT of that species across the interface:[3]

$$I_p = 0.4463 z_i AF c_{bulk} \sqrt{\frac{z_i F}{RT}} \sqrt{\nu} \sqrt{D_i} \qquad \text{(S1)}$$

where z_i is the charge of the transferring species, D_i is the diffusion coefficient of the species, A is surface area of the interface between the two immiscible liquids and ν is scan rate. F, R and T are Faradays constant, the Universal gas constant and temperature, respectively.

In the absence of the AuNP film eq S1 is fulfilled completely for transfer of TMA^+-ions. Using the Randles-Ševčík equation, the diffusion coefficient of TMA^+ in the aqueous phase (D_{TMA^+}) was determined as 11.8 × 10^{-6} cm^2 s^{-1}, in close agreement with previous reports.[4] Addition of AuNPs at the liquid-liquid interface does not alter or influence significantly TMA^+ ions transfer and values of peak current obey the Randles-Ševčík law, except in high scan rates region. However, detailed explanation of that effect is out of scope of the current paper.

The slope of the ion transfer peak current versus the square root of the scan rate is directly proportional to the apparent interfacial area, as not only linear diffusion is involved. Assuming no interactions between TMA^+ and AuNPs (in other words, D_{TMA^+} remains the same with and without), this approach could be used to estimate that about 30% of the interfacial surface area was blocked by AuNPs in both instances. This value corresponds to roughly one half of a hexagonal close packed monolayer of spherical particles (37%), which can be expected based on calculations of the theoretical surface coverage of AuNPs in the nanofilm. The measured coverage is lower because the area available for semi-infinite linear diffusion is higher than the area of the blocking layer itself.

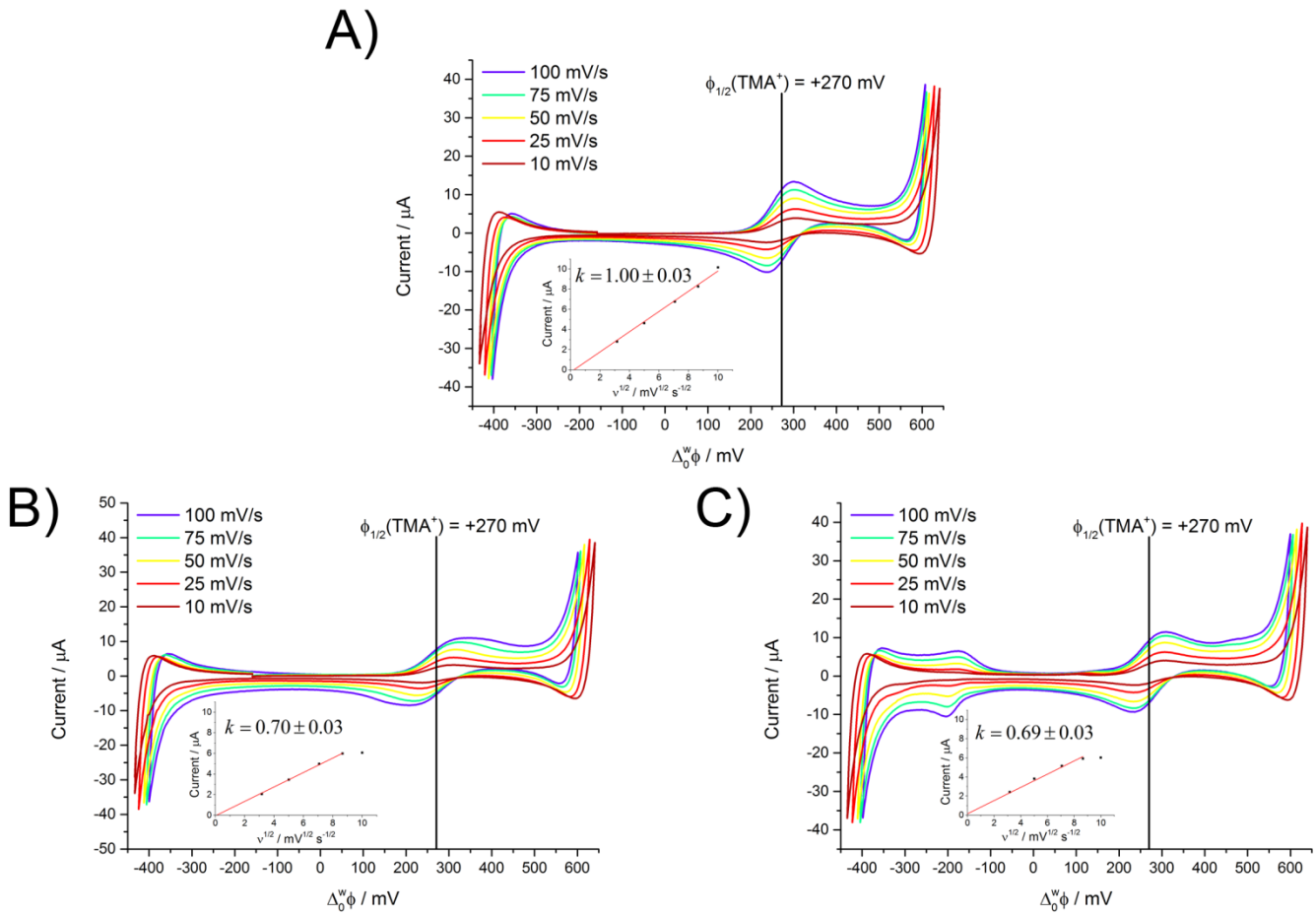

Figure S5. *Ion-transfer CVs (IR compensated) at water│TFT interface with 25 μM TMA^+ in the aqueous phase for following conditions: A) no film, B) 12 nm and C) 38 nm AuNPs films (see cell 1 in Scheme 4B, main text, for comprehensive details of the electrochemical cell configuration).*

SI-4B. Method of Nicholson

In the method of Nicholson,[3] the dimensionless parameter ψ tabulated as the function of the peak separation is directly dependent on the standard electron transfer rate constant k^0.

$$\psi = \frac{\left(\frac{D_O}{D_R}\right)^{\alpha/2} k^0}{\left(\pi D_O \frac{F}{RT} \upsilon\right)^{1/2}} \qquad \text{(S2)}$$

According to the blocked electrode theory, [3] the apparent standard electron transfer rate constant is directly dependent on the surface coverage of the blocking layer θ, and hence the apparent dimensionless parameter of Nicholson can be expressed as

$$\psi_{\text{app}} = \frac{\left(\frac{D_{\text{O}}}{D_{\text{R}}}\right)^{\alpha/2} k^0_{\text{app}}}{\left(\pi D_{\text{O}} \frac{F}{RT} \upsilon\right)^{1/2}} = \frac{\left(\frac{D_{\text{O}}}{D_{\text{R}}}\right)^{\alpha/2} k^0}{\left(\pi D_{\text{O}} \frac{F}{RT} \upsilon\right)^{1/2}} (1-\theta) \qquad \text{(S3)}$$

Facile reaction with a peak-separation of 61 mV has a ψ of 20, so if only one fifth of the interface is active, ψ_{app} becomes 4, corresponding to a peak separation of 66 mV, which is also the experimental peak separation for interfacial electron transfer reactions, as shown in Table 1 in the main text. Of course, this method is very sensitive to any uncompensated resistance, but this rough estimation gives similar surface coverages as determined from ion transfer voltammetry. The blocked electrode theory also explains why significant deviation from expected reversible behavior occurs: as most of the surface area is inactive, peak separation increases with no significant variation in peak currents, as observed experimentally.

SI-5. Standard redox potential of ferrocene in trifluorotoluene

To determine the redox potential of Fc in TFT, firstly the electron transfer potential was measured using the electrochemical cell configuration described in Scheme S1, and shown in Figure S6.

Ag	AgCl	10 mM LiCl 1 mM BACl	0.5 mM Fc 5 mM BATB	10 mM $K_4Fe(CN)_6$ 100 mM $K_4Fe(CN)_6$ 100 mM LiCl	AgCl	Ag
		Ref. Water	Oil	Water		

Scheme S1. Electrochemical cell used in the electron transfer experiment.

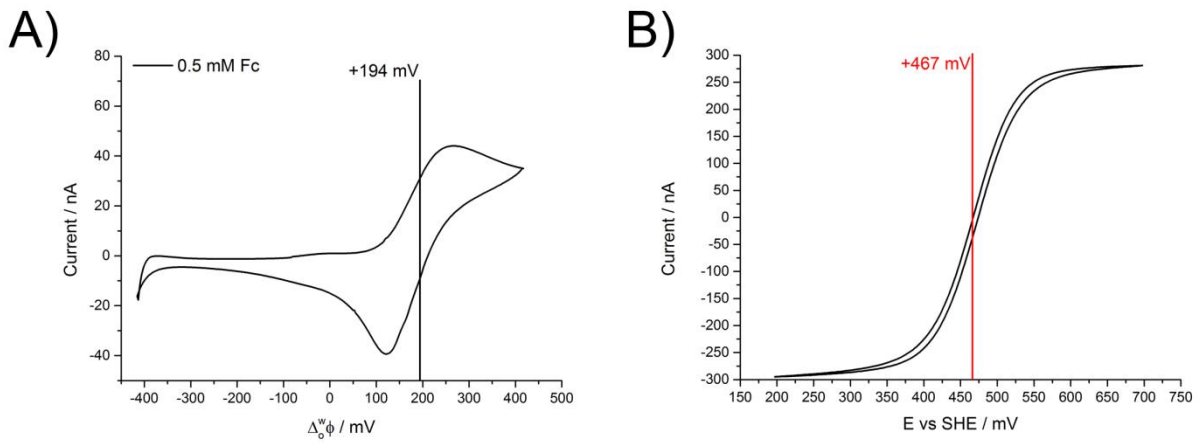

Figure S6. *A) Ion-transfer CV (IR compensated) showing interfacial electron transfer from Fc in oil phase to* $[Fe(CN)_6]^{3-/4-}$ *in aqueous solution. B) Determination of* $E^0(Fe(CN)_6^{3-/4-})$ *by a platinum ultramicroelectrode (25 µm in diameter) in an aqueous solution of 100 mM LiCl.*

Secondly, the redox-potential of $[Fe(CN)_6]^{3-/4-}$ was determined by platinum ultramicroelectrode (25 µm in diameter, RG 6.15) in a 100 mM solution of each salt, with 100 mM LiCl as the supporting electrolyte. The electron transfer potential on the first step can be expressed as described by Fermin and Lahtinen,[5] when the hexacyanoferrate couple in large excess compared to Fc:

$$\Delta_o^w\phi_{et} = E^{0,o}_{Fc^+/Fc} - E^{0',w}_{Fe(CN)_6^{3-}/Fe(CN)_6^{4-}} - \frac{RT}{F}\ln\left(\frac{[Fe(CN)_6^{3-}]}{[Fe(CN)_6^{4-}]}\right) \quad \text{(S4)}$$

Ion-transfer CVs were calibrated, by transfer $TPropA^+$, whose half-wave potential in TFT is equal to –19 mV.

The electron transfer potential for Fc was determined as +194 mV. Thus, taking into account the formal potential of ferro-ferricyanide couple $E^{0',w}_{Fe(CN)_6^{3-}/Fe(CN)_6^{4-}}$ = +0.467 V *vs*. SHE (Fig. S6) and concentration ratio of Fe(II) to Fe(III) of 10 to 100 mM, the final result for $E^{0,o}_{Fc^+/Fc}$ is +720 mV *vs.* aqueous SHE.

SI-6. Supplementary references

1. Haiss, W.; Thanh, N. T. K.; Aveyard, J.; Fernig, D. G. Determination of Size and Concentration of Gold Nanoparticles from UV-Vis Spectra. *Anal. Chem.* **2007**, *79*, 4215–4221.

2. Smirnov, E.; Scanlon, M. D.; Momotenko, D.; Vrubel, H.; Méndez, M. a; Brevet, P.-F.; Girault, H. H. Gold Metal Liquid-Like Droplets. *ACS Nano* **2014**, *8*, 9471–9481.

3. Bard, A. J.; Faulkner, L. R. *Electrochemical Methods: Fundamentals and Applications*; 2nd ed; John Wiley&Sons Inc.: New York, 2001.

4. Koczorowski, Z.; Geblewicz, G. Electrochemical Studies of the Tetrabutyl- and Tetramethyl-ammonium ion Transfer across the Water-1,2-Dichloroethane Interface: A Comparison with the Water—Nitrobenzene Interface *J. Electroanal. Chem.*, **1982**, *139*, 177–191.

5. Fermin D. J.; Lahtinen, R. Dynamic Aspects of Heterogeneous Electron-Transfer Reactions at Liquid-Liquid Interfaces. Iin *Liquid Interfaces in Chemical, Biological, and Pharmaceutical Applications*; Volkov, A. G., Ed.; Marcel Dekker Inc.: New York, 2001, pp. 179–227.